

See discussions, stats, and author profiles for this publication at: <https://www.researchgate.net/publication/257315263>

A Generic Electrospray Classification

Article *in* Journal of Aerosol Science · January 2014

Impact Factor: 2.24 · DOI: 10.1016/j.jaerosci.2013.09.008

CITATIONS

4

READS

40

4 authors, including:



S. Verdoold

Sciver

8 PUBLICATIONS 14 CITATIONS

[SEE PROFILE](#)



Caner U. Yurteri

British American Tobacco

78 PUBLICATIONS 596 CITATIONS

[SEE PROFILE](#)

A generic electrospray classification

S. Verdoold^{a,*}, L.L.F. Agostinho^c, C.U. Yurteri^{b,2}, J.C.M. Marijnissen^{b,1}

^a*Sciver, Wilgenstraat 38, 2861 TP Bergambacht, The Netherlands*

^b*Delft University of Technology, Faculty of Applied Sciences, Julianalaan 67, 2628 BC Delft, The Netherlands*

^c*Wetsus, Agora 1, 8934 CJ Leeuwarden, The Netherlands*

Abstract

One of the major unknown factors when working with electrosprays is the precise spraying mode that is obtained when operating an electrospray. However, as the spraying mode determines to a significant extent the properties of the obtained particles, knowing the spraying mode is crucial for many applications. Currently the spraying modes presented in literature are defined based on optical observations of the liquid meniscus. In a laboratory set-up this approach works fine but in many other situations such an approach is not feasible. For this reason a different approach is developed which uses measurements of the current through an electrospray system to determine the spraying mode of the system. These measurements are relatively simple and can be implemented cost effectively. Although not all spraying modes can be distinguished using this approach, the spraying modes used in most applications can be identified.

Keywords: Electro HydroDynamic Atomization (EHDA), electrospray, spraying mode, classification

Nomenclature

C_{BC}	transferred charge during the development time of a pulse	C
C_{DE}	transferred charge during the relaxation time of a pulse	C
\bar{C}_R	average charge development-relaxation ratio	-
d_{cap}	outer diameter of a capillary	m
$d_{cap,in}$	inner diameter of a capillary	m
G	amplifier gain	-
\bar{I}	mean current	A
$\bar{I}_{min.}$	minimum \bar{I}	A

*Corresponding author

Email address: s.verdoold@sciver.nl (S. Verdoold)

¹Current affiliation: Aerosol Consultancy Marijnissen, Zaart 11, 4819 ED Breda, The Netherlands

²Current affiliation: British American Tobacco, England

K_1	bulk liquid conductivity	S m^{-1}
$N_{\text{ep},i}$	number of extrema in pulse i	-
$\overline{N}_{\text{extr.,p}}$	average number of extrema per pulse	-
p	total number of pulses in the signal	-
P_{DC}	normalised DC-power	-
P_{DLCS}	offset of the linear regression of the DC-corrected and re-normalised cumulative power spectrum density	-
$R_{\text{meas.}}$	measurement resistance	Ω
RSD	relative standard deviation	-
t_{BC}	development time of a pulse	s
t_{DE}	relaxation time of a pulse	s
$\overline{T_R}$	average development-relaxation ratio	-
ΔV	potential difference	V
t	time	s
ϵ	permittivity	$\text{C}^2 \text{ N}^{-1} \text{ m}^{-2}$
σ	standard deviation	-
τ_e	electrical relaxation time	s

1. Introduction

Due to its extraordinary properties the number of applications using Electro-Hydrodynamic Atomisation (EHDA) has increased dramatically during the last decades. EHDA, sometimes called electrospraying, is among many other things applied in crop spraying (Geerse, 2003), the creation of emulsions (Abu-Ali & Barringer, 2005), the creation of thin films (Jaworek, 2007) and the production of particles with a very specific size and/or composition (Borra et al., 1997, 1998; Camelot, 1999; DePaoli et al., 2003; Ciach, 2006; Enayati et al., 2010; Yurteri et al., 2010). The technique is also widely used as a soft but efficient ionisation technique in mass spectrometry set-ups (Dülcks & Juraschek, 1999; Cech & Enke, 2001; Wei et al., 2002). The wide variety in applications together with their rather different requirements illustrate the versatility of the technique. For correct operation of all applications it is however crucial that the electrospraying happens in a well-defined way.

It is well known that the behaviour of an electrospray depends strongly on the electric field it experiences, the material properties of the used liquid, the electrode geometry and other boundary conditions. In literature a number of classifications have been proposed to distinguish between the various spray situations (Cloupeau & Prunet-Foch, 1990, 1994; Grace & Marijnissen, 1994; Juraschek & Röllgen, 1998; Jaworek & Krupa, 1999). These classifications are mainly based on visual observations of the liquid meniscus. Together with a

mapping of the effect of experimental conditions like the applied liquid flow rate and the applied electric field, these classifications are helpful in getting the wanted electrospray behaviour. However, when using those classifications, it remains necessary to check whether a certain spraying “mode” was obtained. For real-life and/or up-scaled applications, this often becomes unpractical and/or expensive so a different approach is needed.

It was found that for the geometries and liquid flow rates often used in mass spectrometry set-ups, the current through the system and the behaviour of the liquid meniscus are correlated Juraschek & Röllgen (1998); Cech & Enke (2001); Wei et al. (2002); Marginean et al. (2007). A similar observation was made for unforced nano-electrosprays (Alexander et al., 2006; Paine et al., 2007; Alexander, 2008). These correlations seem to be specific for a given liquid and configuration. It should also be noted that both a mass spectrometry and an unforced nano-electrospray set-up employ a relatively small nozzle (typically $\lesssim 200 \mu\text{m}$) and relatively low flow rates (typically $\lesssim 0.1 \text{ mL h}^{-1}$). The effect of larger nozzle diameters and/or higher flow rates on the correlation remains to be investigated.

Here it is attempted to find a general mapping between the properties of the current through the system and the spraying mode that is independent of the material properties of the liquid, the electrode geometry and other experimental conditions. To accomplish this, it is assumed that a change in the liquid meniscus is “directly” reflected as a change in the current through the system and that a change in the current reflects a change in the liquid meniscus. As a result analysing the current characteristics is an (indirect) way to analyse the behaviour of the meniscus that may be used to classify the various spraying modes. The assumed relation between the meniscus and the current through the system has already been shown to be valid for systems with a small nozzle diameter and relatively low flow rates (Juraschek & Röllgen, 1998; Alexander et al., 2006; Marginean et al., 2007). For systems with larger nozzles and higher flow rates the amount of (semiconducting) liquid close to the nozzle will be significantly larger in many cases. For this type of systems the validity of the assumption has not been shown yet. However, the electrical relaxation time, τ_e , defined as

$$\tau_e = \frac{\epsilon}{K_1} \quad (1)$$

with ϵ being the permittivity of the liquid and K_1 being the bulk liquid conductivity, is rather small for most liquids used in electrospraying. Together with the limited amount of liquid per spray system, it can be expected that even for the larger systems changes in the liquid meniscus are “directly” reflected in the currents through the system, especially when the currents are measured close to the liquid meniscus. Experimental validation is however still needed.

2. Experimental set-up and techniques

The experimental set-up used in this study is shown schematically in figure 1. In the experiments a syringe pump (Harvard, PHD2000) was used to pump liquid through a nozzle at flow rates in the range of 0.1 mL h^{-1} to 10 mL h^{-1} . A number of different nozzles were used, all with outer diameters $\geq 0.71 \text{ mm}$. In order to ensure that the currents were measured close to the liquid meniscus, all nozzles were made of conducting (metallic) materials and the current

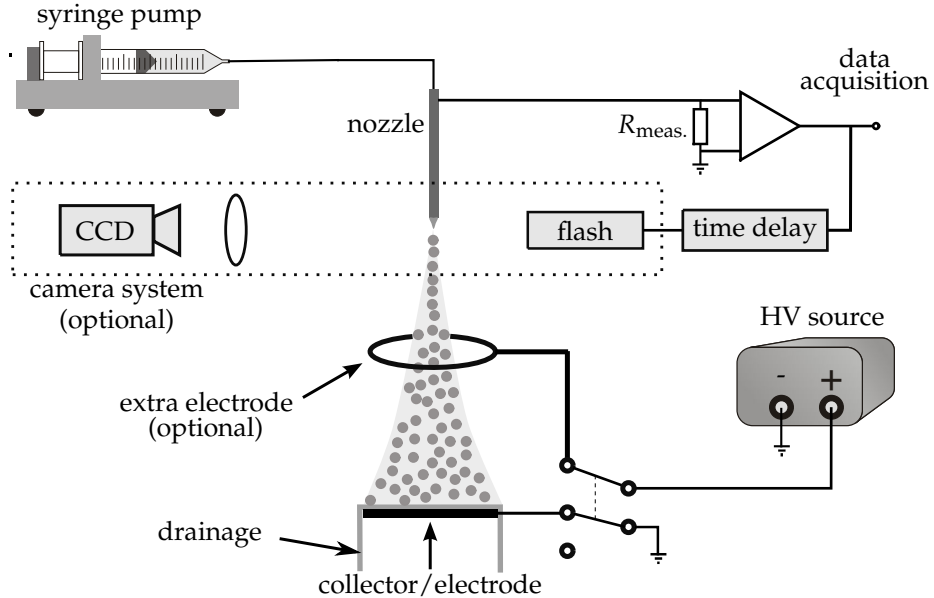


Figure 1: Schematic representation of the set-up. Liquid was pumped through a metallic nozzle by a syringe pump. By applying a high potential to either the collector plate or an optional ring electrode an electrospray system was created. The current through the system was measured at the nozzle side and optionally used to trigger a camera system.

measurements were performed at the nozzle. At some distance from the nozzle a conducting collector plate was located onto which the created droplets deposited. In some experiments a ring electrode was placed between the nozzle and the collector plate. An electric field was created by applying a high electric potential to either the collector or the ring electrode. When a ring electrode was used, the collector was kept at ground potential. Figure 2 gives an schematic overview of the various nozzle-ring-plate combinations that were used. The main difference between the “needle type” (Type I and II) and the “nozzle type” (Type III and IV) nozzles is the ratio of the inner and outer diameter of the nozzle. For the needle type nozzles the inner diameter, $d_{\text{cap,in}}$, is comparable to the outer diameter, d_{cap} , whereas the nozzle type nozzles have an inner diameter of 0.2 mm which is significantly smaller than d_{cap} for the nozzles used in the current experiments. This leads to rather different situations close to the nozzle tip for both generic types. Together with the extra ring electrode used in a number of configurations, it is clear that the electric fields in the configurations differ significantly, leading to a different spraying behaviour. In all configurations the development of the liquid meniscus will however be reflected in the measured current through the system. A generic classification based on this current should therefore be valid for all configurations. For convenience table 1 gives an overview of the used configurations. It should be noted that by varying the the liquid, the applied liquid flow rate and the applied potentials, each configuration can be used for a variety of experiments.

In order to avoid liquid from building up on the flat collector, a thin sheet of tissue was draped over the collector to drain possible excess liquid.

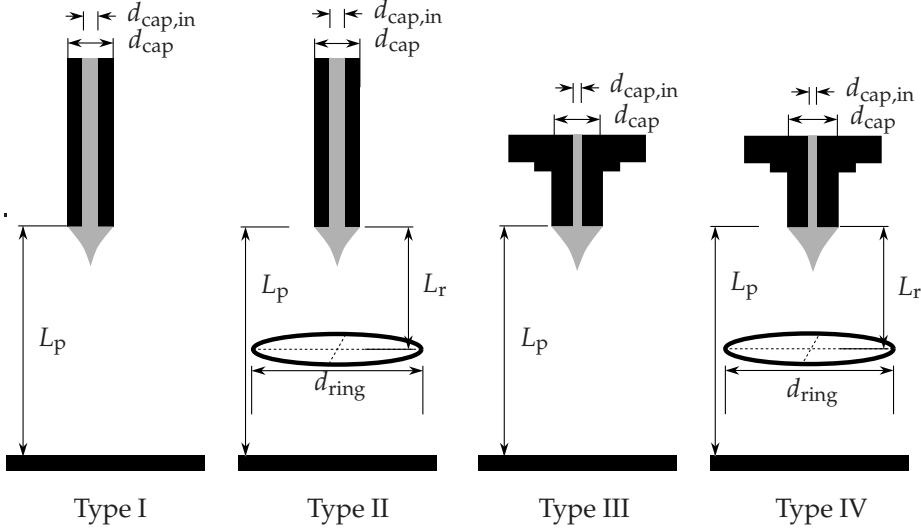


Figure 2: A schematic overview of the electrospray configuration types used.

Config.	Type	d_{cap} [mm]	$d_{\text{cap,in}}$ [mm]	L_p [mm]	d_{ring} [mm]	L_r [mm]	$R_{\text{meas.}}$ [Ω]	G [-]
1	II	0.91	0.61	11	20	70	11450	500 \times
2	I	0.91	0.61	27	-	-	11460	500 \times
3	II	0.91	0.61	61	20	12	11460	500 \times
4	III	2.00	0.20	15	-	-	11460	100 \times
5	IV	2.00	0.20	58	20	12	1147	500 \times
6	IV	8.00	0.20	65	20	15	1147	500 \times
7	I	0.71	0.41	24	-	-	46800	10 \times
8	I	0.91	0.61	22	-	-	1147	500 \times
9	II	1.83	1.55	47	20	12	1147	500 \times
10	I	0.71	0.41	30	-	-	1×10^6	1 \times
11	II	1.65	1.37	47	20	12	11460	100 \times
12	I	0.91	0.61	30	-	-	9760	500 \times
13	III	2.00	0.20	30	-	-	9760	10 \times
14	III	2.00	0.20	30	-	-	9760	100 \times
15	IV	2.00	0.20	70	20	15	9760	100 \times

Table 1: The configurations used in this research. In this paper only results of a subset of the configurations are presented. In each configuration the liquid, its flow rate and the applied potential can still be freely adjusted. The optional ring electrodes were toroidal of shape with a major radius equal to $\frac{1}{2} \cdot d_{\text{ring}}$ and a minor radius of approximately 1 mm.

2.1. Signal acquisition

The current through the spray system was measured by a differential amplifier (Burr-Brown, INA 110KP) monitoring the voltage across a resistor ($R_{\text{meas.}}$) placed between the nozzle and ground potential. Both the amplifier gain (G) and the value of the measurement resistor could be changed in order to achieve an optimum regarding measurement accuracy and the introduced (and amplified) thermal noise (Verdoold, 2012). Moreover the measurement resistance was always intentionally kept relatively small ($< 99.7 \text{ k}\Omega$) to minimise its influence on the spraying behaviour.

The amplified signals were recorded by either a storage oscilloscope (LeCroy 9354) or a computer-based data acquisition card. The sample rates varied but were always $> 5 \text{ kHz}$ to ensure that the most relevant parts of the signal were captured (Parvin et al., 2005; Stachewicz et al., 2009). A number of experiments were performed at sample rates up to 2.5 MHz . These experiments were performed using a different storage oscilloscope (LeCroy WavePro 960XL) and a different differential amplifier (LeCroy DA1822A). The results from these experiments confirmed that sampling at 5 kHz is sufficient to capture the most relevant parts of the signal.

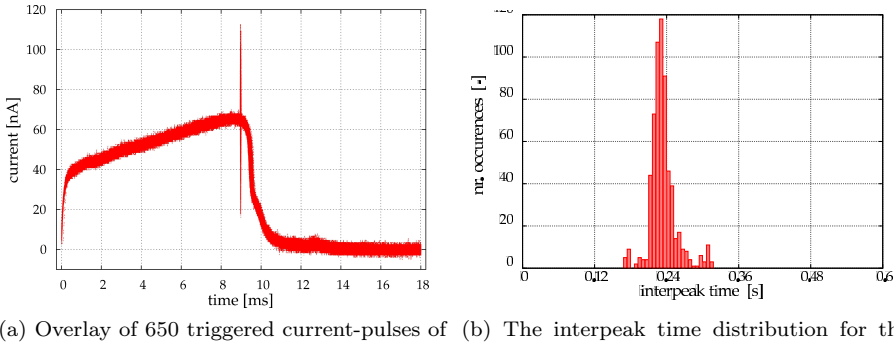
The temperature dependent offset of the differential amplifier was determined before each measurement series and subtracted from the recorded signal. A possible 50 Hz component was removed from the signal using a digital notch filter.

2.2. Image acquisition

In a part of the experiments the liquid meniscus was observed using an optical system consisting of a CCD camera (Kodak Megaplus ES 1.0), a long-distance microscope (Infinity, model K2 Long-Distance Microscope) and an illumination system (Oxford Laser, HSI1000 fast illumination system). Using the measured currents and a variable time delay to trigger the optical system enabled to visualise the liquid meniscus at various moments during a pulsating current. For stable pulsating signals this makes it possible to create a series of snapshots for a complete cycle, for other signals snapshots of the beginning of a cycle will not be available due to the small delay in the illumination (order of $5 \mu\text{s}$) and the camera (order of $20 \mu\text{s}$) see for example figures 4a and 4b. The electrospray set-up was attached to a traversal system. By traversing the complete spray system relative to the optical system, the snapshots could be taken at different distances from the nozzle. For stable pulsating spray systems this made it possible to reconstruct multi exposed, high resolution images of the complete spray situation from nozzle to counter electrode at any given moment in the cycle of the liquid emission process (see for example figure 6a). The system was always allowed to stabilise for at least a minute after each change to the system and each traversal.

3. Correlation between liquid meniscus and current characteristic

To investigate a possible correlation between the liquid meniscus and the simultaneously measured current through the system, the camera system described in section 2 was used. As this camera system was triggered by the measured current signal a possible correlation was most easily determined for



(a) Overlay of 650 triggered current-pulses of a typical stable pulsating electrospray. (b) The interpeak time distribution for the system that was used in figure 3a.

Figure 3: Overlay of 650 triggered current pulses of a typical stable pulsating electrospray together with the corresponding distribution of the inter-peak times.

spraying modes having a heavily pulsed current characteristic. For modes like the cone-jet mode the current characteristic is rather constant and reproducible triggering becomes difficult (see also Cloupeau & Prunet-Foch (1994); Grace & Marijnissen (1994); Jaworek & Krupa (1999)). However, adjusting the triggering level in these cases enables to trigger “arbitrarily” which confirmed the reported observations that these modes exhibit a nearly constant meniscus and current characteristic. For the pulsating systems the response time of the electronics made it impossible to determine the correlation at the beginning of a pulse. Assuming the signal to be stable enables to get around this problem by triggering on a pulse and taking images of the next pulse. The validity of this assumption needs to be confirmed.

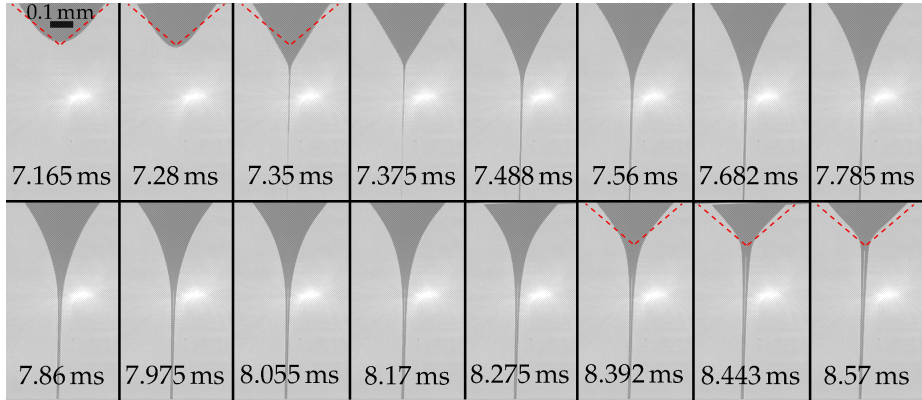
3.1. Stability of pulsating systems

To verify the stability of a typical pulsating electrospray the pulses of the corresponding current characteristic were compared with each other. Figure 3a shows some typical results for a Configuration 1 geometry spraying ethanol with an applied potential difference of $\Delta V = 4.50$ kV. From this figure it is clear that for a stable pulsating electrospray all pulses are nearly identical.

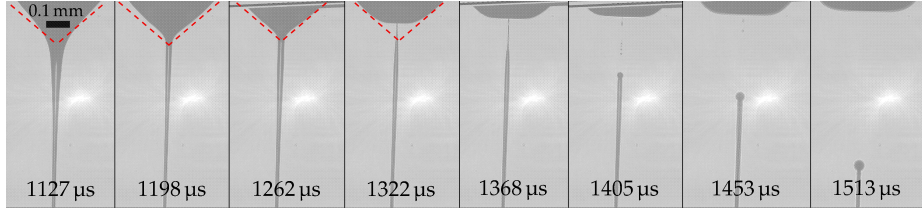
Figure 3b shows that the system was nearly stable with a pulsation frequency of approximately 4.3 Hz. Extended measurement series revealed that during these measurements spanning a couple of hours the pulsation frequency slowly changed from 3.5 Hz to 5 Hz. The time-scale of this change is however much larger than the time between two consecutive pulses. Hence triggering on a certain pulse and using a relatively large delay to image the liquid meniscus at the onset of the next pulse is a valid way to gain insight in the development of the meniscus during the onset of a current pulse. The double spike around 9 ms is present in all pulses and originates from the flash light source needed for the image acquisition.

3.2. Liquid meniscus vs measured current

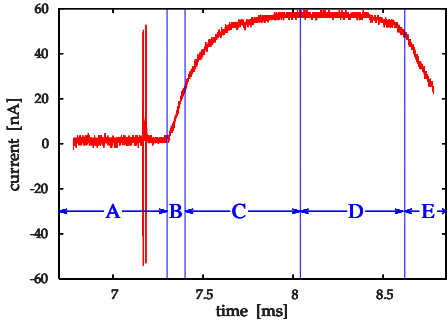
Synchronised measurements of both the liquid meniscus and the current through the system may be used to determine whether a correlation exists between the behaviour of the meniscus and the measured current. Figure 4



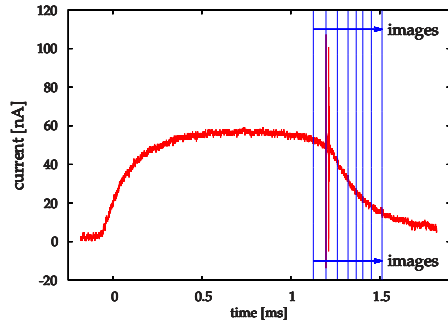
(a) The tip of the liquid meniscus at the start of the periodic current-pulse as shown in 4c. The optical system was triggered using the previous pulse. The dashed lines in some of the images depict the outline of a cone with the Taylor angle (49.3°).



(b) The tip of the liquid meniscus at the end of the periodic current-pulse as shown in 4d. The optical system was triggered using the beginning of the pulse. The dashed lines in some of the images depict the outline of a cone with the Taylor angle (49.3°).



(c) The current-pulse following the trigger pulse (corresponds with the images in 4a). The letters denote the various stages in the pulse development (the vertical lines correspond with the stage boundaries).



(d) Typical current-signal used for both triggering the system and acquiring images of the liquid meniscus (the vertical lines correspond with the images of figure 4b).

Figure 4: The tip of the liquid meniscus at various moments during a pulse in the current through the system together with the corresponding characteristic pulses.

shows for example the tip of the liquid meniscus just below the nozzle outlet together with the current through the system for a similar electrospray system as described in the previous section (Configuration 1, spraying ethanol with $\Delta V = 4.50 \text{ kV}$ and a flow rate of 2 mL h^{-1}). To some of the images the contour of a cone with an angle of 49.3° (the equilibrium cone angle of a charged droplet in an electric field without liquid flow, Taylor (1964)) is added. Figures 4a and 4c show results for the largest part of the current-pulse. To accomplish this, the system was triggered on the preceding pulse which due to the stable signal delivered reliable results. Figure 4b shows the results for the last part of the pulse. The corresponding current-pulse is shown in figure 4d for the complete pulse. The results shown in both 4b and 4d correspond to the very same pulse that was used to trigger the acquisition system. This improved the accuracy of the results and is reflected in the different timings for both image sequences (0 ms represents the triggering moment).

Comparing figures 4c and 4d with figure 3a it is clear that although the same spray systems were used (the same geometries using the same parameters) the pulse durations differ significantly. Within each separate measurement series the pulses match however closely, indicating that the systems were just spraying in a different spraying mode. The cause of the different spraying mode is not known. Most likely the different modes originate from slight differences in the operational history of the system and/or in minimal differences in the system geometry.

The double spikes in figures 4a and 4c originate from the firing of the flash light used in the camera system (which was operated in double exposure mode). Comparing the images with the current signal reveals that the current only increases significantly when liquid is emitted from the meniscus. Before the onset point (around 7.3 ms in this case) the shape of the meniscus does change but this is not reflected in the measured current. At the onset of the pulse the meniscus very rapidly transforms to a cone shape and liquid is emitted in a fine jet. In some of the images the Taylor angle is denoted by the dashed lines. From these lines it seems that around the moment that liquid starts/stops being emitted, the meniscus resembles the classical Taylor cone the most (around 7.165 ms in figure 4a and around 1.262 ms in figure 4b).

3.2.1. Pulsation stages

To get a better overview of the development of the meniscus during a current-pulse it is illustrative to look at the shape of the meniscus at various moments. The contours of the meniscus for the results of figure 4a and 4c are depicted in figure 5. In this figure the contours are grouped together to emphasise the similarities and differences at various moments during a pulse. These similarities and differences can then be used to define a number of stages in the meniscus development and gain more insight in the system. Each group contains a contour of the previous and the next group to make comparing consecutive groups easier.

In the “pre-onset stage” (“A”, $\lesssim 7.3 \text{ ms}$) region the meniscus changes significantly but no cone-jet like meniscus (Jaworek & Krupa (1999); Cloupeau & Prunet-Foch (1994)) is observed and no significant current is measured. This is different for the “onset-stage” (“B”, $\lesssim 7.42 \text{ ms}$). In this stage a cone-jet is observed and the measured current through the system increases at a constant rate. After the relatively short “onset-stage” the “development stage” (“C”, $\lesssim 8.04 \text{ ms}$) starts in which the measured current keeps increasing. However, the rate with

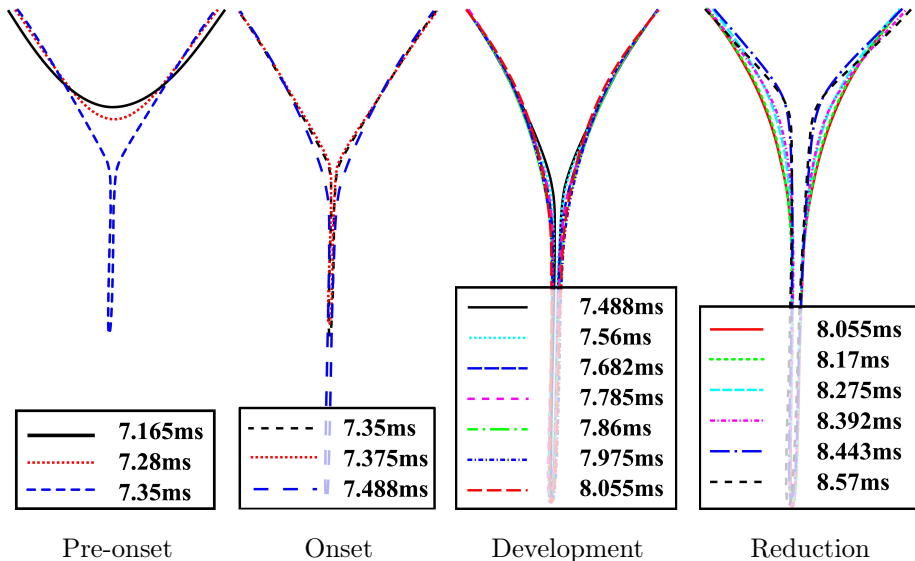


Figure 5: The contours of the tip of the liquid meniscus of figure 4 for various moments during a pulsation. The contours are grouped together to illustrate the meniscus behaviour at various moments during a pulse.

which the current increases decreases throughout the complete stage leading to a maximum measured current at the end of the stage. Looking at the corresponding contours it can be seen that the increasing current is accompanied by an increase in the jet diameter.

In the “reduction stage” (“D”, $\gtrsim 8.04$ ms) the opposite behaviour occurs: the jet becomes smaller as function of time and the current decreases. Just before the end of this stage the resemblance of the meniscus with the classical Taylor cone increases (figure 4a). Looking at figure 4c it can be seen that the rate with which the current decreases at the end of the pulse varies considerably and exhibits a sudden change around 8.62 ms.

To investigate this sudden change more accurately, images of the tip of the meniscus at the end of the current pulse were made while triggering on the start of the same current pulse. This improved accuracy by reducing the variance due to slightly different pulse durations. The results are shown in figure 4b. As already mentioned, with a slightly decreasing current as function of time the jet gets smaller and the meniscus as a whole resembles the classical Taylor cone more and more. This is illustrated by the dashed lines in the first images. From figure 4d it can be seen that around 1.25 ms a sudden change in the rate of decrease of the current is present. Although this moment is not exactly captured by the images in figure 4b, it seems the sudden change coincides with the moment the meniscus closely resembles a classical Taylor cone which is just before the jet detaches from the meniscus. From that moment on (so for $\gtrsim 1.25$ ms in figure 4d or $\gtrsim 8.62$ ms in figure 4c) the system enters the “relaxation stage” (“E”). In this stage the current-characteristic exhibits a shape which resembles the charge/discharge characteristic of a capacitor.

From figures 4 and 5 it can be seen that during the complete “development stage” and most of the “reduction stage” a cone-jet system is present, albeit

with changing cone dimensions. So a cone-jet-like system is present during a large part of the pulse duration. For a steady cone-jet spraying mode various scaling laws have been presented in literature relating the current through the complete system, which equals the current through the cone in the absence of discharges, to material properties and the applied flow rate (Fernández De La Mora & Loscertales, 1994; Gañán-Calvo et al., 1997; Hartman et al., 1999; Yurteri et al., 2010).

3.3. Spraying mode vs measured current

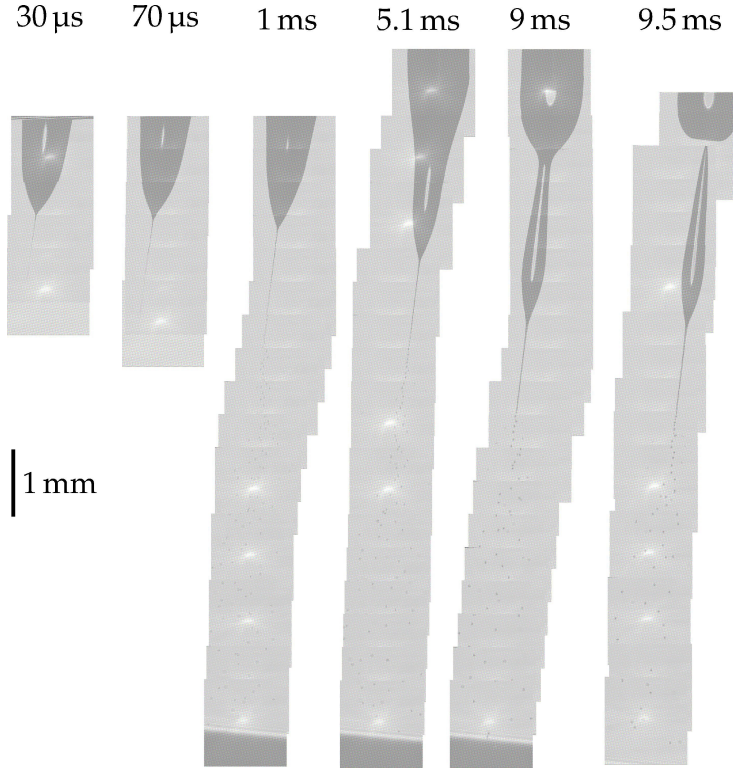
As already mentioned in section 2.2 it is possible for stable electrosprays to combine triggered and delayed image acquisition with a traversing system. By systematically scanning the area between the nozzle and the counter electrodes it then becomes possible to reconstruct the complete spray situation for arbitrary delays relative to the pulse onsets/trigger level.

Figure 6 shows such a reconstruction for the experiments of figure 3a (Configuration 1 spraying ethanol with $\Delta V = 4.50 \text{ kV}$ and a flow rate of 2 mL h^{-1}). In this reconstruction the vertical displacements of the individual images were based on the vertical displacements of the traversal system. The horizontal displacements were chosen to “match” in order to compensate for slight misalignments (the spray systems were not spraying exactly in the vertical direction).

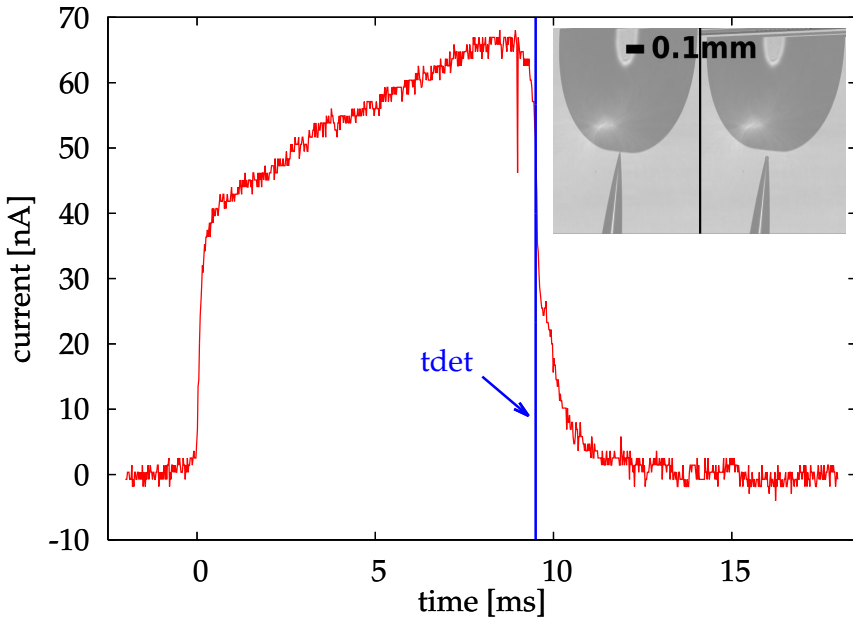
The decreasing side of the characteristic pulse consists of two parts. It starts with a fast dropping part followed by a slightly more modest current decrease. This behaviour is observed for all pulses shown in figure 3a. Combining the reconstructed images with the current characteristics it is tempting to conclude that the more modest current drop starts when the elongated droplet actually detaches from the liquid meniscus. This is affirmed by the inset of figure 6b which shows some double exposed images at 9.500 ms and 9.520 ms from the trigger. However, due to the variability of the pulse duration (see figure 3a) the moment of the jet detachment cannot be determined accurately enough for these measurements to validate this assumption.

The reconstructed images reveal that the system was spraying in the spindle mode whereas kind of an intermittent-cone (Cloupeau & Prunet-Foch (1994)) was obtained during the experiments depicted in figure 4. This was clearly reflected in a totally different characteristic current-pulse. Especially in the development stage the current-characteristic shows a rather different behaviour. Although in figure 6 the tip of the meniscus is rather far away from the place where the actual detachment of the liquid takes place, the correlation between the measured current and the liquid meniscus seems to be present in this case as well. The pulse duration and the relative duration of the development and the reduction stage also differ significantly for the different spraying modes. Hence, the current through the system and especially its development in time reveals information about the spraying mode of those systems.

Figure 7 shows the current through the system and the corresponding liquid menisci at specified moments for a number of spraying modes that have been reported in literature. From this figure it is clear that the correlation between the meniscus and the current is present for all pulsating modes except when hardly any current is measured (Configuration 12, “Dripping” mode). As expected, a nearly constant current is obtained when a cone-jet with either varicose breakup or kink instabilities (see Jaworek & Krupa (1999) and Cloupeau & Prunet-Foch (1994)) is observed. The current characteristic for the kink breakup seems to



(a) Reconstructed, multi-exposed images of the spray system for a number of delays after the onset of the current pulse.



(b) Typical current-pulse present during the experiments of figure 6a. The spike around 9 ms originates from the illumination system. The inset shows the liquid meniscus at 9.500 ms and 9.520 ms from the triggering moment ($\Delta t = 20 \mu s$).

Figure 6: The reconstructed spray system for various moments during a current-pulse.

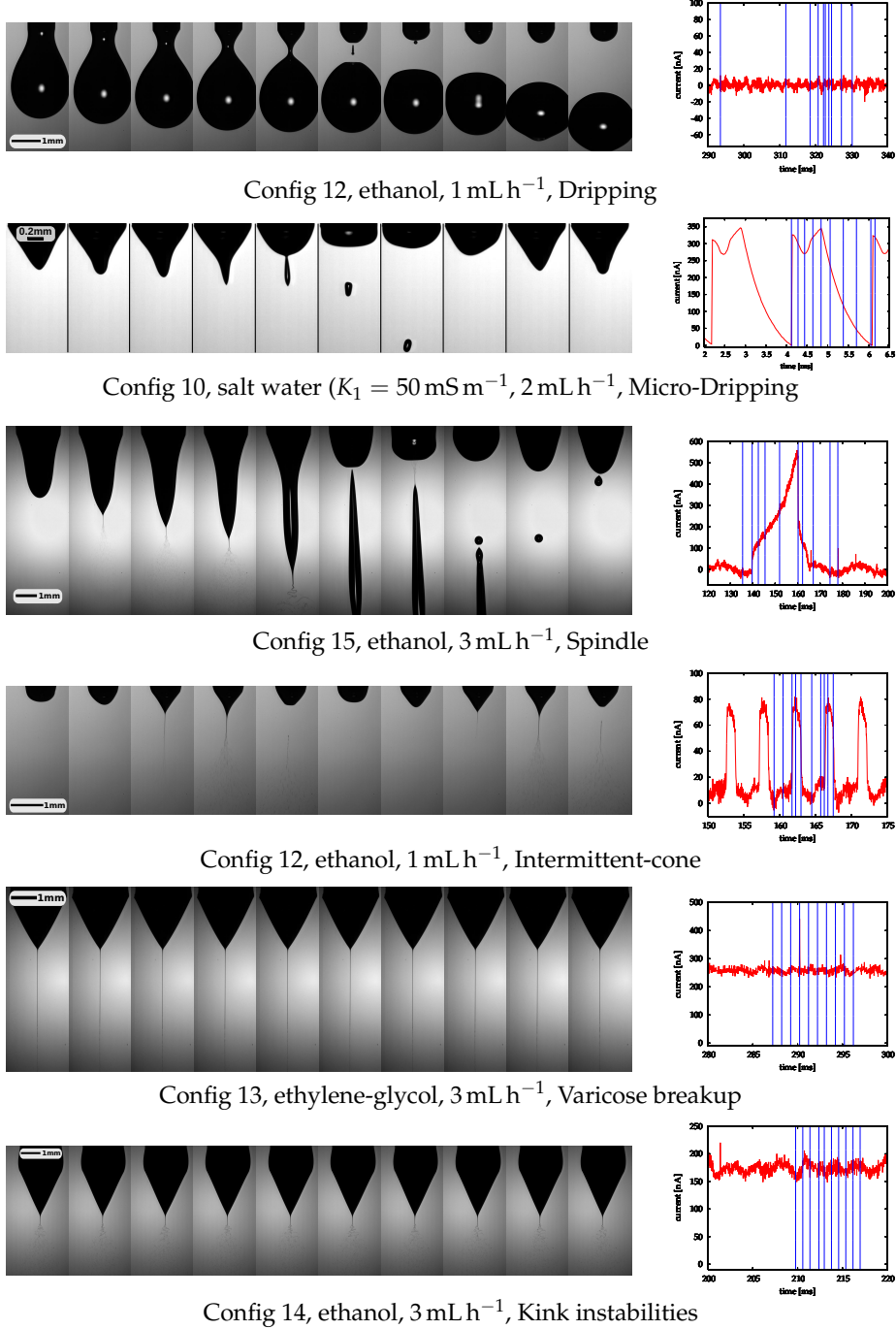


Figure 7: Liquid menisci and currents through the systems for systems exhibiting a number of spraying modes. The moments the images were taken are indicated by the added vertical lines in the current characteristics.

have a larger variability than the characteristic for varicose breakup. This may enable to discriminate between both modes based on the current characteristics. More focussed research is however needed to confirm or falsify this.

In the results for Configuration 10 with a flow rate of 2 mL h^{-1} a “dip” is seen right after the onset of the current pulse. Such a “dip” was only seen for systems in a dripping mode and the relative magnitude and visibility depends on the material properties and the used geometry. Hence the shape of the pulse may be used to discriminate between the pulsating modes.

4. Current characteristics

The spraying behaviour of an electrospray systems depends on many factors like for example the geometry, polarity, material properties, occurring discharges etcetera which is reflected in the measured currents. As a result the measured currents can be rather different. This is illustrated by figure 8 which shows a number of typical current characteristics together with the experimental conditions from which they were obtained. A classification based purely on the currents through the system should be able to deal with all these types of characteristics. Hence a number of summarising characteristic numbers are identified which describe the properties of the signal adequately. A combination of those characteristic numbers can then be used to classify the main spraying modes. Subclasses like varicose and whipping breakup (kink instabilities) may not always be distinguishable using this approach as they are based on events occurring away from the nozzle.

The current-signal was analysed both in the time and the frequency domain, leading to characteristic numbers for both domains. It should be stressed that both methods are just a different way of describing the behaviour of the same data. Due to the nature of the processing steps, it is important that a possible amplifier offset is always removed from the data before the actual processing takes place.

4.1. Time domain characteristic numbers

4.1.1. DC-current, \overline{I}

Because of its well-defined properties, the cone-jet mode is the most used spraying mode for real-life applications. This spraying mode has been the subject of many theoretical and experimental investigations. It has been shown that in this mode the current through the system mainly depends on liquid properties, the liquid flow rate the applied electric field strength and the geometry (Gañán-Calvo et al., 1997; Hartman, 1998; Hartman et al., 1999; Gañán-Calvo, 1999; Gañán-Calvo, 2004; Yurteri et al., 2010). As a result the DC-current is a valuable characteristic number when spraying in the cone-jet mode.

The DC-current, or the average value of the current, \bar{I} is determined easily. It is however a rather crude approximation of the signal because it simply averages it. Hence it is possible that a pulsating signal has the same \bar{I} as a cone-jet mode with the same liquid, geometry etc.. In such a situation it is impossible to discriminate between both situations based on \bar{I} without extra knowledge. So even though \bar{I} can be very useful when the spraying mode is already known, its usefulness in determining the spraying mode is limited without extra knowledge.

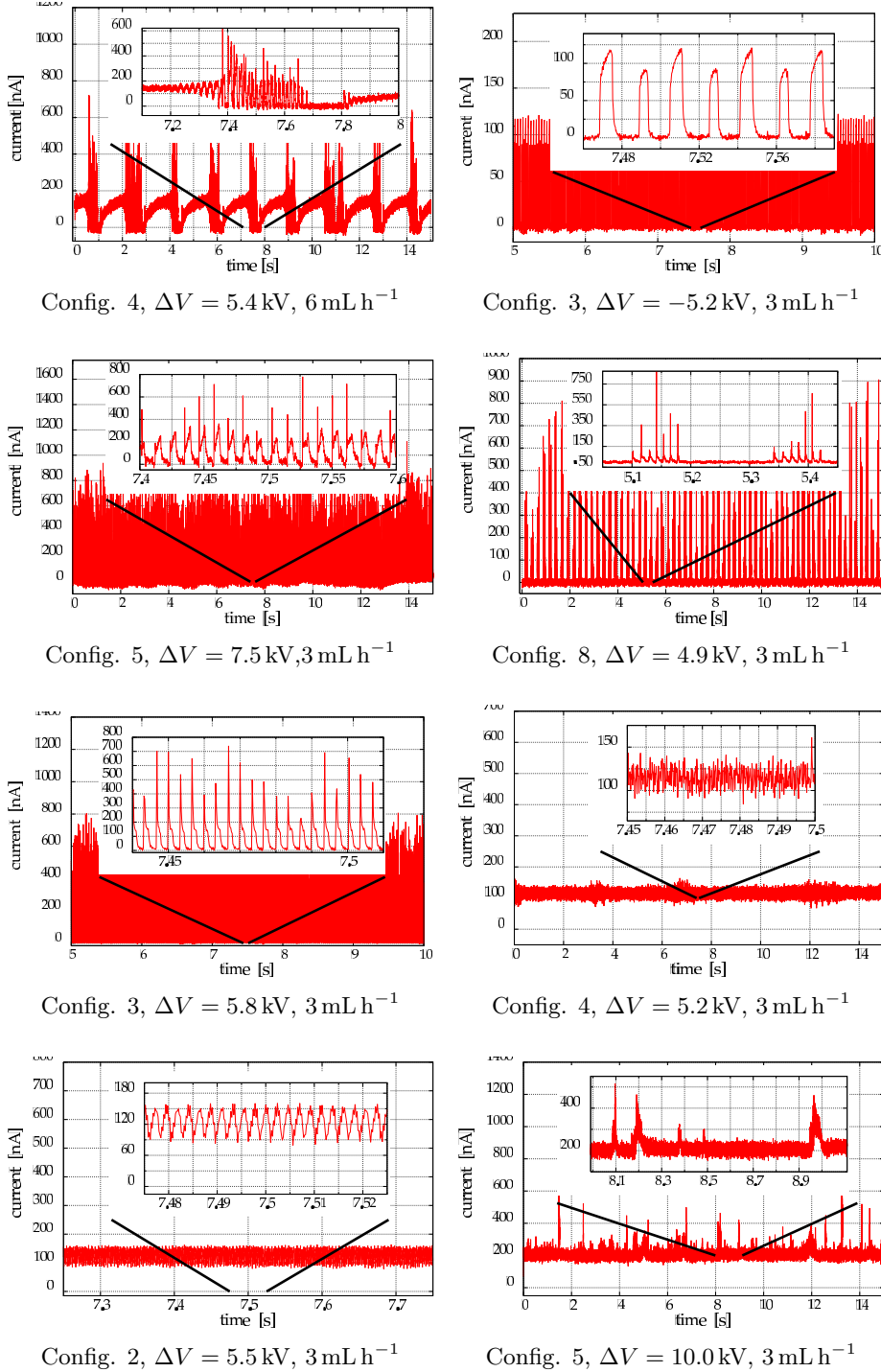


Figure 8: Some typical currents through an EHDA system. Except for the characteristics of Configuration 8 which was obtained spraying ethylene glycol all characteristics were obtained using ethanol.

For this reason this research only uses \bar{I} to determine whether spraying with charge transfer occurs at all ($\bar{I} > 0$).

The acquired data will contain some noise and there will often be a very small inaccuracy in the determination of the amplifier offset. Hence it is assumed that spraying occurs when $\bar{I} > \bar{I}_{\min.}$ with $\bar{I}_{\min.} > 0$. For the data discussed here, $\bar{I}_{\min.} > 5 \text{ nA}$ was found to be appropriate (see for example figure 8, Configuration 3, $\Delta V = -5.2 \text{ kV}$ and figure 9). This value is very close to the minimum current through a cone-jet system for the liquids used in this research (see Gañán-Calvo et al. (1994, 2013)). As long as the $\bar{I}_{\min.}$ -value is smaller than or equal to this minimum current this gives an extra confirmation that with $\bar{I} \leq \bar{I}_{\min.}$ the system will for sure not be in a cone-jet mode.

4.1.2. (absolute value of) Relative standard deviation, $|\frac{\sigma}{\bar{I}}|$

The variability of the current differs significantly between the various spraying modes. The relative standard deviation, RSD, defined as $\frac{\sigma}{\bar{I}}$ with σ being the standard deviation, is a natural way to describe this.

For situations in which only a small number of relatively small peaks are observed above the baseline \bar{I} may become a very small negative value due to the always present inaccuracies in the determination of the amplifier offset. This may result in wildly fluctuating RSD-values for those modes. To avoid this the absolute value of $|\bar{I}|$ (which corresponds to using the absolute value of the relative standard deviation) was used in this research. See figure 9 for some typical results.

4.1.3. Mean-median ratio, $\frac{|\bar{I}|}{|\tilde{I}|}$

The relative amount of peaks and the area of the peaks (which is effectively the amount of charge emitted during the occurrence of the peak) seems to be significantly different for the various spraying modes. To get an indication of the amount of peaks in the signal the mean-median ratio, defined as $\frac{|\bar{I}|}{|\tilde{I}|}$, is used with \tilde{I} being the median of the signal values. In the absence of any peaks the ratio will be ≈ 1 , and the ratio increases with an increasing number of (relatively large) peaks. When the number of peaks increases such that the peaks make up more than half the signal, the median will also start to increase with an increasing number of peaks and the ratio starts decreasing towards 1.

The limited accuracy in the determination of the amplifier offset may lead to very small, negative values for \bar{I} and/or \tilde{I} in situations where a small electric field is applied. To avoid problems due to this, absolute values of both the mean and the median are taken before the ratio is determined. Some typical results are given in figure 9.

4.1.4. Average development-relaxation ratios, $\overline{C_R}$ and $\overline{T_R}$

In section 3.2 it was found that for spraying modes resulting in a pulsed current, the pulse shape differs significantly between different spraying modes and various stages in the development of a pulse were identified. The boundaries between two consecutive stages may sometimes be difficult to determine objectively, especially for an arbitrary signal. Hence certain stages (see figure 4c) were combined to arrive at an objective characteristic number that is easy to determine. This leads to a development stage (consisting of stages “B” and “C”) and a relaxation stage (consisting of stages “D” and “E”). The ratios of

either the duration of the development and the relaxation stages, $\frac{t_{BC}}{t_{DE}}$, or the amount of charge transferred during those stages, $\frac{C_{BC}}{C_{DE}}$, provide global information about the situation at the liquid meniscus without knowledge about the exact meniscus shape.

Mild discharges may be present on top of the pulses in a pulsating system (figure 8, Configuration 5, $\Delta V = 7.5 \text{ kV}$). These discharges will often form the maximum current-value in a pulse while they are only present for a very short period compared to the pulse duration. Without extra precautions, such discharges have a large influence on the $\frac{t_{BC}}{t_{DE}}$ and $\frac{C_{BC}}{C_{DE}}$ ratios even when the rest of the pulses remains the same. To avoid this the location of the maximum values of the pulses were determined using a smoothed version of the signal thereby reducing the influence of the “fast” discharge peaks. Using this “location-information” of the maximum value, the original, non-smoothed signal was used to determine the various characteristic numbers. For signals containing strong discharges the smoothing approach may not be sufficient. Using higher sampling rates may help in those situations but this was not explored in this research.

The amount of charge transferred during the individual stages depends among other things on the conductivity and other material properties of the liquid. Because the complete pulse originates from exactly the same system, it is assumed that the material properties are the same for all stages of the pulse. As long as the factors influencing the current through the system are independent of the actual current value, the $\frac{C_{BC}}{C_{DE}}$ ratio can be used as a characteristic number. As $\frac{C_{BC}}{C_{DE}}$ (areas) takes the shape of the pulse into account it may be preferred over $\frac{t_{BC}}{t_{DE}}$ (times).

A pulsed signal contains many pulses and $\frac{t_{BC}}{t_{DE}}$ and $\frac{C_{BC}}{C_{DE}}$ may be slightly different for each pulse. Hence the arithmetic mean of the values of all individual pulses in the signal, given by

$$\overline{C_R} = \frac{1}{p} \sum_{i=1}^p \frac{C_{BC}}{C_{DE}} \Big|_i \quad (2)$$

and

$$\overline{T_R} = \frac{1}{p} \sum_{i=1}^p \frac{t_{BC}}{t_{DE}} \Big|_i \quad (3)$$

where p is the total number of pulses in the signal, is thought to be representative for the complete signal. Some typical results for $\overline{C_R}$ are shown in figure 9.

4.1.5. Average number of extrema per pulse, $\overline{N_{\text{extr.,p}}}$

As mentioned in section 3.3 the current pulses of a system in micro-dripping mode exhibits a very typical shape. After an initial current increase marking the start of the pulse, a dip is seen followed by a further more or less smooth increase of the current (see for example figure 7, Configuration 10). This behaviour was only seen by the authors for systems in “dripping-mode” (Cloupeau & Prunet-Foch (1994); Jaworek & Krupa (1999)). Determining the number of extrema in a pulse is an efficient way to find a possible dip in the signal (a pulse containing a dip contains at least 3 extrema). In case of a noisy signal some low-pass filters may however be necessary to get reliable results: if “noise-ripples” are interpreted as small peaks they will introduce a large number of extrema. To

describe the complete signal, all pulses need to be located and individually analysed after which the results of all individual pulses are used to describe the complete signal. In this case, the arithmetic mean of the number of extrema in the pulses, $\overline{N}_{\text{extr.,p}}$, was used, leading to

$$\overline{N}_{\text{extr.,p}} = \frac{1}{p} \sum_{i=1}^p N_{\text{ep},i} \quad (4)$$

where $N_{\text{ep},i}$ is the number of extrema for pulse i . Figure 9 shows some typical results.

4.2. Frequency domain characteristic numbers

In order to analyse the signal in the frequency domain, the normalised Power Spectral Density (PSD) of the signal was considered. The normalised PSD gives the relative amount of power in the signal as function of the frequency and can be used to determine the strongest frequency components in the signal. It can be determined using various techniques, but it is important that the resulting spectral resolution is sufficiently high. Using a low spectral resolution may influence the obtained results. A minimum value for the spectral resolution is arbitrary and may depend on the actual signals being processed. For all data treated here a spectral resolution of 0.25 Hz was found to be appropriate.

4.2.1. Normalised DC-power, P_{DC}

The DC-power, P_{DC} , of the signal is the power of the non-periodic components of the signal relative to the total power in the signal. Hence its values will be rather different for pulsating and nearly constant signals, which may help in discriminating between the spraying modes. P_{DC} corresponds to the 0 Hz component of the PSD.

It is important to remember that the P_{DC} -values give the *relative* power of the constant components. Signals with a significant periodicity on top of a strong DC-component may despite the periodicity still have a rather large P_{DC} due to this property. Even though the periodicity will still influence the P_{DC} -value in such a case, its influence will decrease with increasing DC-component. This should be kept in mind when interpreting the data based on P_{DC} . It also explains why it is crucial that the amplifier offset is carefully removed when P_{DC} is used to discriminate between pulsating and continuous spraying modes. See figure 9 for some typical values.

4.2.2. Intercept of the linear regression of the DC-corrected, rescaled cumulative spectrum, P_{DLCS}

When high fields are applied discharges may start to occur. This results in sharp peaks in the current signal and an increased variability of the signal values. However, the appearance of slower pulsations in the signal leads to an increased variability as well.

The main difference between the slower pulsations and the fast discharges is that for a stable pulsating signal the slower pulsations occur at a rather well defined frequency whereas the discharges may occur at seemingly random intervals. This is clearly reflected in the normalised cumulative power spectrum densities of the signals: more or less regular pulsations result in a step in the

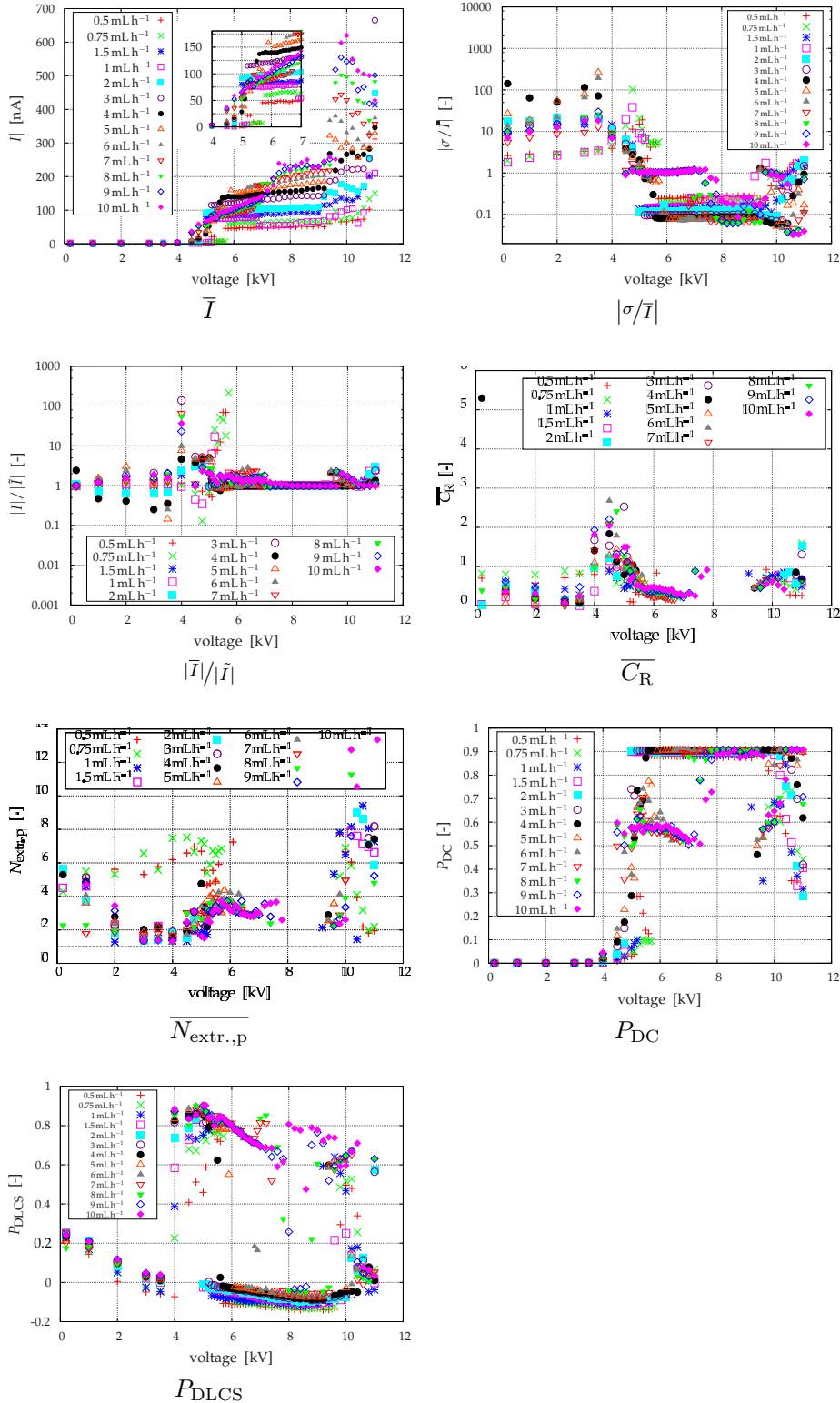


Figure 9: Typical processing results for the characteristics of sections 4.1 and 4.2 for a configuration 4 (Type III) system spraying ethanol.

cumulative PSD whereas irregular discharges lead to an almost linear behaviour of the cumulative PSD. A linear regression of the normalised cumulative PSD can be used to summarise it with two numbers. Because the slope of such a regression is related to the sampling frequency of the data and as a result is not ideally suited for generic purposes, the intercept of the regression was selected as a potential characteristic number. However, using a cumulative PSD the DC-component will have a significant influence on the results of the linear regression. This component does not contain any information about the fluctuations of the signal so it only obscures the parts related to the variations in the signal. Hence the linear regression is applied to the cumulative PSD from which the DC-component is subtracted and which is then rescaled or normalised to obtain values in the region [0, 1]. This way the focus is on the fluctuating parts of the signal and the results can be compared between different measurements and configurations. The intercept of this regression, P_{DLCS} , is used as characteristic number. Its values are an indication of the relative importance of the “random” parts of the signal. Figure 9 shows some typical values.

4.3. Systematic overview

To get more insight in the current characteristics for the various spraying modes, systematic series of measurements were performed for several configurations, liquid flow rates and material properties. For each combination the applied potentials were varied stepwise from 0 kV to a maximum potential of V_{max} and for each applied potential the current through the system was recorded. Such series encompass all or just a number of the possible spraying modes. Regular visual observations were used to determine the actual spraying modes roughly. To avoid measuring transitional effects, a stabilisation period of at least 60 s was used between consecutive measurements. See Verdoold (2012) for more details.

All measured currents were processed to determine the corresponding characteristic numbers described in sections 4.1 and 4.2. These characteristic numbers were then plotted as function of the applied potential. Some typical results are shown in figure 9 which gives the results for a configuration 4 system spraying ethanol.

5. Classification

The characteristic numbers treated in sections 4.1 and 4.2 only provide information about a single measurement. To be able to distinguish between several spraying modes the systematic approach as described in section 4.3 was used. Some typical results are shown in figure 9 for a single configuration. From this figure it is clear that general trends seem to be present. Similar trends were observed for the other configurations that were analysed using the same approach (see Verdoold (2012) for more details). Together with the actual current characteristics, visual observations and results from literature it was investigated whether generic trends are present that can be related to the actual spraying modes.

It was found that even though $|\bar{I}|$ is very useful when spraying in a cone-jet mode, it cannot be used to unambiguously distinguish between the cone-jet mode and some other modes. Hence $|\bar{I}|$ was only used to determine whether a

significant current is flowing through the system or whether its value originates from noise in the measurements. A value of 5 nA was found to be appropriate as boundary value (figure 8, Configuration 3, $\Delta V = -5.2$ kV and figure 9). Below this value the system is for sure in a dripping mode. For $|\frac{\sigma}{\bar{I}}| > 2.5$ the system is in a dripping mode, while $|\frac{\sigma}{\bar{I}}| < 0.5$ indicates that the system exhibits a nearly constant signal. Intermediate values of $|\frac{\sigma}{\bar{I}}|$ indicate a pulsating mode which encompasses a number of spraying modes. For $0.9 < \frac{|\bar{I}|}{|\bar{I}|} < 1.1$ a relatively smooth, nearly constant current is obtained while for $\frac{|\bar{I}|}{|\bar{I}|} \leq 0.9$ and $\frac{|\bar{I}|}{|\bar{I}|} \geq 1.1$ pulsating signals or signals with relatively strong discharge peaks are present.

Two characteristic numbers were treated based on the shape of individual pulses (sections 4.1.4 and 4.1.5). These numbers can only be used to discriminate between the various pulsating modes. $\overline{C_R}$ describes the pulse shape based on the charge transport before and after it reaches its maximum value. It was found that for $\overline{C_R} \gtrsim 3.5$ the pulse shapes have the characteristic shape as present when an electrospray system is in the spindle mode. For $\overline{C_R} \lesssim 3.5$ the pulses have the characteristic shape of the intermittent cone mode. An exact limiting value is hard to determine because similar $\overline{C_R}$ -values may be obtained for both spraying modes when different experimental conditions are applied (envision for example the pulse of figure 6b on the same time-scale as the pulses in figure 4). Based on the available experimental results a value of 3.5 was found to be appropriate.

The average number of extrema per pulse, $\overline{N_{extr.,p}}$, counts the number of times the rate of change of the current changes sign during a pulse. This was done on a smoothed version of each pulse to minimise the influence of measurement noise and discharges. Some results are shown in figure 9. It was found that for $\overline{N_{extr.,p}} > 2.75$ the systems are in a dripping mode. Distinguishing between a dripping and a micro-dripping mode is difficult using the proposed characteristic numbers. However, also in the existing classifications the boundary between them is not clearly delimited. In general $|\bar{I}|$ will be larger for a micro-dripping mode and $|\frac{\sigma}{\bar{I}}|$ is larger for a dripping mode. Hence it was decided that for a dripping mode $|\bar{I}| \leq 5$ nA and $|\frac{\sigma}{\bar{I}}| > 2.5$ while for a micro-dripping mode $|\bar{I}| > 5$ nA and $|\frac{\sigma}{\bar{I}}| < 2.5$. Of course these boundary conditions are relatively arbitrary. More focussed research is needed to determine them more accurately.

In sections 4.2.1 and 4.2.2 two characteristic numbers were proposed which consider the data in the frequency domain. It was found that the DC-power, P_{DC} , can be used for similar purposes as $|\frac{\sigma}{\bar{I}}|$: when $0.2 < P_{DC} \leq 0.75$ the system is in a pulsating mode or in a (heavily) distorted continuous mode and for $P_{DC} > 0.75$ the system is in a nearly constant mode, possibly with small disturbances (figure 8, Configuration 5, $\Delta V = 10.0$ kV and figure 9). Depending on the other processing steps that are performed on the signal, the determination of P_{DC} may be faster than the determination of $|\frac{\sigma}{\bar{I}}|$.

The other frequency domain characteristic number, P_{DLCS} , was created to get more insight in the fluctuating part of the signal. It was found that for the systems through which hardly any current is flowing P_{DLCS} is small (typically < 0.25). Similar values are obtained for systems in a cone-jet mode: in such system P_{DLCS} is typically < 0.2 . As soon as a pulsation occurs in the signal P_{DLCS} increases significantly towards a value of 1. It seems that P_{DLCS} is even more sensitive to a small number of pulses in the signal than $|\frac{\sigma}{\bar{I}}|$. This

may enable to distinguish between the cone-jet sub-modes “varicose breakup” and “kink instabilities” as kink instabilities are expected to lead to a slightly increased variation of the current through the system. More research is however needed to confirm or falsify this.

Increased values for P_{DLCS} ([0.25, 1]) are obtained for pulsating modes without significant discharges. When (strong) discharges start influencing the signal and/or the pulsation frequencies become such that each pulse in the time domain contains only a very limited number of points, this leads to lower values for P_{DLCS} . An increasing amount and/or strength of the discharges or an increasing pulsation frequency lowers P_{DLCS} even further. This may enable to determine whether the proposed classification is applicable or not: When heavily distorted signals or signals containing strong discharges are present, some of the characteristic numbers cannot be determined or do no make sense and the classification is not applicable. In such cases the P_{DLCS} -values become smaller. As mentioned above such P_{DLCS} -values are however not unique for heavily distorted signals so additional criteria have to be used.

Discharges will in general increase the current through the system and decrease the relative importance of the constant component. Hence attention was at first focussed at \bar{I} and P_{DC} . It was found that for the signals containing discharges a significant current is going through the system whereas the current is much smaller for the low field-strength (“dripping -like”) signals. A boundary value for $|\bar{I}|$ is hard to determine generically. Based on the available data it was found that a value of 5 nA gives a satisfactory separation between both situations. In the current context the exact value is however not crucial, so using a slightly larger value is also fine. With cone-jet modes (the other situation in which P_{DLCS} becomes small) it was found that P_{DC} becomes relatively large compared to the other situations, typically > 0.75 .

Using a combination of $|\bar{I}|$, P_{DC} and P_{DLCS} it then becomes possible to determine whether the proposed classification method is applicable or whether the signal is just too “wild” and/or contains too many discharges: when $P_{DLCS} < 0.6$ and $P_{DC} < 0.75$ and $|\bar{I}| > 5$ nA it is very likely that either a mixture of spraying modes or a spraying mode that cannot yet be classified by this method is being considered.

Table 2: Overview of the proposed classification and a number of classifications reported in literature. The corresponding behaviour of the liquid meniscus can be found in for example Verdoold (2012), Jaworek & Krupa (1999) or Cloupeau & Prunet-Foch (1994). The $N_{\text{extr},\text{p}}$ and C_R values can only be determined for pulsating current-characteristics.

Type	Juraschek & Röllgen (1998)	Cloupeau & (1990)	Jaworek & Krupa (1999)	Characteristics
Pulsating	-	Dripping	Dripping	$ \bar{I} \leq 5 \text{nA}$ $ \frac{\sigma}{\bar{I}} > 2.5$ $\overline{N_{\text{extr},\text{p}}} > 2.75$ $ \bar{I} < 0.9 \vee \frac{ \bar{I} }{P_{\text{DC}}} > 1.1$ $P_{\text{DC}} < 0.2$
Pulsating	Axial I	-	-	not enough data available
Pulsating	Axial II	Micro-dripping	Micro-dripping	$ \bar{I} > 5 \text{nA}$ $0.5 < \frac{\sigma}{\bar{I}} < 2.5$ $\overline{N_{\text{extr},\text{p}}} > 2.75$
Pulsating	Axial II	Spindle	Spindle	$ \bar{I} < 0.9 \vee \frac{ \bar{I} }{P_{\text{DC}}} > 1.1$ $\overline{C_R} > 3.5$
Pulsating	Axial II	Intermittent cone	-	$0.2 < P_{\text{DC}} < 0.75$ $P_{\text{DLCS}} > 0.2$ $\overline{C_R} < 3.5$ $\overline{N_{\text{extr},\text{p}}} < 2.75$
Pulsating	Axial II	-	Multi- spindle	no data available
Continuous	Axial III	Cone-jet varicose breakup	Cone-Jet	$ \bar{I} > 5 \text{nA}$ $ \frac{\sigma}{\bar{I}} < 0.5$ $P_{\text{DC}} > 0.75$ $0.9 < \frac{ \bar{I} }{P_{\text{DC}}} < 1.1$ $P_{\text{DLCS}} < 0.2$

Type	Juraschek & Röllgen (1998)	Cloupeau & Prunet-Foch (1990)	Jaworek & Krupa (1999)	Characteristics
Continuous	Axial III	Cone-Jet kink instabilities	Cone-Jet	$P_{DLCS} < 0.3$ ³
Continuous	Non-axial	Cone-Jet kink instabilities	Precessing	no data available
Continuous	Non-axial	Cone-Jet kink instabilities	Oscillating	no data available
Continuous	Axial III	Simple jet	-	no data available
Continuous	Non-axial	Ramified jet	Ramified jet	no data available
Continuous	Non-axial	Rim emission	-	no data available
Continuous	Non-axial	Multi-jet	Multi-jet	no data available
Continuous	Non-axial	-	Ramified meniscus	no data available

³This value is based on a limited number of data. More focussed research may be needed to determine it more accurately.

Table 2 summarises the results of the foregoing in its last column. The other columns show the corresponding classification schemes presented in literature by other authors. The corresponding behaviour of the liquid meniscus for the various modes is illustrated in various places, see for example Verdoold (2012), Jaworek & Krupa (1999) or Cloupeau & Prunet-Foch (1994). For a number of spraying modes no data was available and the table entries were left empty. In some cases like for example for the precessing and the oscillating mode it might be that the current characteristics of these modes are very similar to those of the “cone-jet varicose break-up” and “cone-jet kink instabilities” modes. Actual measured data is however needed to confirm this. For the continuous modes in which liquid leaves the meniscus simultaneously from multiple points things are even less predictable. For the “simple jet” or “multi-jet” the measured signals may still contain useful information. With the “rim emission”, “ramified jet” or “ramified meniscus” modes the measured signals probably just become very irregular leading to small P_{DLCS} values. Actual measured data is however crucial to check those assumptions, so the corresponding table entries were left empty.

6. Conclusions

The behaviour of the liquid meniscus of an electrospray system is reflected rather accurately in the current through that system. This can be used to determine the spraying mode of the system by processing the current through the system. Several characteristic numbers can be identified that describe the behaviour of the current through the system. It was found that each individual characteristic number is not sufficient to classify the spraying mode by itself. However, a combination of those numbers does enable to classify the spraying mode.

The used characteristic numbers do not include any material properties and make no (implicit) assumptions about the used geometries. Hence the resulting classification is generic. An overview of the classification is given in table 2. Most non-axial spraying modes may not be recognised as such because the measurements discussed here were only performed at the nozzle. The spraying modes most often used in practical situations can however be classified using this approach. Together with the simplicity of the required measurements and the fact that no optical access to the spray systems is needed, makes this generic classification a valuable tool for most set-ups employing electrosprays.

References

- Abu-Ali, J., & Barringer, S. (2005). Method for electrostatic atomization of emulsions in an ehd system. *Journal of Electrostatics*, 63, 361–369.
- Alexander, M. S. (2008). Pulsating electrospray modes at the liquid-liquid interface. *Appl. Phys. Lett.*, 92, 144102–3.
- Alexander, M. S., Paine, M. D., & Stark, J. P. W. (2006). Pulsation modes and the effect of applied voltage on current and flow rate in nanoelectrospray. *Analytical Chemistry*, 78, 2658–2664.

- Borra, J.-P., Camelot, D., Chou, K.-L., Kooyman, P. J., Marijnissen, J. C. M., & Scarlett, B. (1998). Bipolar coagulation for powder production: Micro-mixing inside droplets. *Journal of Aerosol Science*, *30*, 945–958.
- Borra, J.-P., Camelot, D., Marijnissen, J. C. M., & Scarlett, B. (1997). A new production process of powders with defined properties by electrohydrodynamic atomization of liquids and post-production electrical mixing. *Journal of electrostatics*, *40/41*, 633–638.
- Camelot, D. (1999). *The bipolar coagulation process for powder production*. Ph.D. thesis Delft University of Technology.
- Cech, N. B., & Enke, C. G. (2001). Practical implications of some recent studies in electrospray ionization fundamentals. *Mass Spectrometry Reviews*, *20*, 362–387.
- Ciach, T. (2006). Microencapsulation of drugs by electro-hydro-dynamic atomization. *International Journal of Pharmaceutics*, *324*, 51–55.
- Cloupeau, M., & Prunet-Foch, B. (1990). Electrostatic spraying of liquids: Main functioning modes. *Journal of Electrostatics*, *25*, 165–184.
- Cloupeau, M., & Prunet-Foch, B. (1994). Electrohydrodynamic spraying functioning modes: a critical review. *J. Aerosol Sci*, *25*, 1021–1036.
- DePaoli, D. W., Tsouris, C., & Hu, M. Z. C. (2003). Ehd micromixing reactor for particle synthesis. *Powder Technology*, *135-136*, 302–309.
- Dülcks, T., & Juraschek, R. (1999). Electrospray as an ionisation method for mass spectrometry. *Journal of Aerosol Science*, *30*, 927 – 943.
- Enayati, M., Chang, M.-W., Bragman, F., Edirisinghe, M., & Stride, E. (2010). Electrohydrodynamic preparation of particles, capsules and bubbles for biomedical engineering applications. *Colloids and Surfaces A: Physicochemical and Engineering Aspects, In Press, Corrected Proof*, –.
- Fernández De La Mora, J., & Loscertales, I. G. (1994). The current emitted by highly conducting taylor cones. *Journal of Fluid Mechanics*, *260*, 155–184.
- Gañán-Calvo, A., Dávila, J., & Barrero, A. (1997). Current and droplet size in the electrospraying of liquids. scaling laws. *Journal of Aerosol Science*, *28*, 249–275.
- Gañán-Calvo, A. M. (2004). On the general scaling theory for electrospraying. *Journal of Fluid Mechanics*, *507*, 203–212a.
- Gañán-Calvo, A., Lasheras, J., Dávila, J., & Barrero, A. (1994). The electrostatic spray emitted from an electrified conical meniscus. *Journal of Aerosol Science*, *25*, 1121 – 1142. doi:[http://dx.doi.org/10.1016/0021-8502\(94\)90205-4](http://dx.doi.org/10.1016/0021-8502(94)90205-4).
- Gañán-Calvo, A. M. (1999). The surface charge in electrospraying: it's nature and its universal scalings laws. *Journal of Aerosol Science*, *30*, 863–872.

- Gañán-Calvo, A. M., Rebollo-Muñoz, N., & Montanero, J. M. (2013). The minimum or natural rate of flow and droplet size ejected by taylor cone-jets: physical symmetries and scaling laws. *New Journal of Physics*, 15, 033035.
- Geerse, K. B. (2003). *Applications of electrospray: from people to plants*. Ph.D. thesis Delft University of Technology.
- Grace, J. M., & Marijnissen, J. C. M. (1994). A review of liquid atomization by electrical means. *Journal of Aerosol Science*, 25, 1005–1019.
- Hartman, R. (1998). *Electrohydrodynamic atomization in the cone-jet mode, From Physical Modeling to powder production*. Ph.D. thesis Delft University of Technology.
- Hartman, R. P. A., Brunner, D. J., Camelot, D. M. A., Marijnissen, J. C. M., & Scarlett, B. (1999). Electrohydrodynamic atomization in the cone-jet mode physical modeling of the liquid cone and jet. *Journal of Aerosol Science*, 30, 823–849.
- Jaworek, A. (2007). Electrospray droplet sources for thin film deposition. *Journal of Materials Science*, 42, 266–297.
- Jaworek, A., & Krupa, A. (1999). Classification of the modes of ehd spraying. *Journal of Aerosol Science*, 30, 873–893.
- Juraschek, R., & Röllgen, F. (1998). Pulsation phenomena during electrospray ionization. *International Journal of Mass Spectrometry*, (pp. 1–15).
- Marginean, I., Nemes, P., & Vertes, A. (2007). Astable regime in electrosprays. *Phys. Rev. E*, 76, 026320–6.
- Paine, M. D., Alexander, M. S., & Stark, J. P. (2007). Nozzle and liquid effects on the spray modes in nanoelectrospray. *Journal of Colloid and Interface Science*, 305, 111–123.
- Parvin, L., Galicia, M. C., Gauntt, J. M., Carney, L. M., Nguyen, A. B., Park, E., Heffernan, L., & Vertes, A. (2005). Electrospray diagnostics by fourier analysis of current oscillations and fast imaging. *Analytical Chemistry*, 77, 3908–3915.
- Stachewicz, U., Dijksman, J. F., Burdinski, D., Yurteri, C. U., & Marijnissen, J. C. M. (2009). Relaxation times in single event electrospraying controlled by nozzle front surface modification. *Langmuir*, 25, 2540–2549.
- Taylor, G. (1964). Disintegration of water drops in an electric field. *Proceedings of the Royal Society of London. Series A. Mathematical and Physical Sciences*, 280, 383–397.
- Verdoold, S. (2012). *ElectroHydroDynamic Atomisation - Unipolar and bipolar characterisation and modelling*. Ph.D. thesis Delft University of Technology. doi:<http://dx.doi.org/10.4233/uuid:863b8d50-f39c-4543-8f9e-410833a1bd56>.

- Wei, J., Shui, W., Zhou, F., Lu, Y., Chen, K., Xu, G., & Yang, P. (2002). Naturally and externally pulsed electrospray. *Mass Spectrometry Reviews*, 21, 148–162.
- Yurteri, C., Hartman, R., & Marijnissen, J. (2010). Producing pharmaceutical particles via electrospraying with an emphasis on nano and nano structured particles - a review. *KONA Powder and Particle Journal*, 28, 91–115.

List of Figures

1	Schematic representation of the set-up. Liquid was pumped through a metallic nozzle by a syringe pump. By applying a high potential to either the collector plate or an optional ring electrode an electrospray system was created. The current through the system was measured at the nozzle side and optionally used to trigger a camera system.	4
2	A schematic overview of the electrospray configuration types used.	5
3	Overlay of 650 triggered current pulses of a typical stable pulsating electrospray together with the corresponding distribution of the inter-peak times.	7
4	The tip of the liquid meniscus at various moments during a pulse in the current through the system together with the corresponding characteristic pulses.	8
5	The contours of the tip of the liquid meniscus of figure 4 for various moments during a pulsation. The contours are grouped together to illustrate the meniscus behaviour at various moments during a pulse.	10
6	The reconstructed spray system for various moments during a current-pulse.	12
7	Liquid menisci and currents through the systems for systems exhibiting a number of spraying modes. The moments the images were taken are indicated by the added vertical lines in the current characteristics.	13
8	Some typical currents through an EHDA system. Except for the characteristics of Configuration 8 which was obtained spraying ethylene glycol all characteristics were obtained using ethanol. . . .	15
9	Typical processing results for the characteristics of sections 4.1 and 4.2 for a configuration 4 (Type III) system spraying ethanol. . . .	19

List of Tables

1	The configurations used in this research. In this paper only results of a subset of the configurations are presented. In each configuration the liquid, its flow rate and the applied potential can still be freely adjusted. The optional ring electrodes were toroidal of shape with a major radius equal to $\frac{1}{2} \cdot d_{\text{ring}}$ and a minor radius of approximately 1 mm.	5
2	Overview of the proposed classification and a number of classifications reported in literature. The corresponding behaviour of the liquid meniscus can be found in for example Verdoold (2012), Jaworek & Krupa (1999) or Cloupeau & Prunet-Foch (1994). The $\overline{N}_{\text{extr.,p}}$ and C_R values can only be determined for pulsating current-characteristics.	23